AGU PUBLICATIONS

JGR

Journal of Geophysical Research: Solid Earth

RESEARCH ARTICLE

10.1002/2013JB010451

**Key Points:**
- Seasonal deformation in the Himalaya is induced by continental water storage
- Seasonal displacements computed for half-space; layered spherical elastic Earth
- Importance of realistic Earth structure to model seasonal displacements

**Supporting Information:**
- Figures S1–S3

**Correspondence to:**
K. Chanard,
kristel.chanard@gmail.com

**Citation:**
Chanard, K., J. P. Avouac, G. Ramillien, and J. Genrich (2014), Modeling deformation induced by seasonal variations of continental water in the Himalaya region: Sensitivity to Earth elastic structure, *J. Geophys. Res. Solid Earth*, *119*, 5097–5113, doi:10.1002/2013JB010451.

Received 27 JUN 2013
Accepted 8 APR 2014
Accepted article online 12 APR 2014
Published online 6 JUN 2014

# Modeling deformation induced by seasonal variations of continental water in the Himalaya region: Sensitivity to Earth elastic structure

**K. Chanard[1,2], J. P. Avouac[1], G. Ramillien[3], and J. Genrich[1]**

[1]Tectonics Observatory, Geology and Planetary Sciences Division, California Institute of Technology, Pasadena, California, USA, [2]Laboratoire de Géologie, Ecole Normale Supérieure, Paris, France, [3]Géophysique Environnement Toulouse, Toulouse, France

**Abstract** Strong seasonal variations of horizontal and vertical positions are observed on GPS time series from stations located in Nepal, India, and Tibet (China). We show that this geodetic deformation can be explained by seasonal variations of continental water storage driven by the monsoon. For this purpose, we use satellite data from the Gravity Recovery and Climate Experiment to determine the time evolution of surface loading. We compute the expected geodetic deformation assuming a perfectly elastic Earth model. We consider Green's functions, describing the surface deformation response to a point load, for an elastic homogeneous half-space model and for a layered nonrotating spherical Earth model based on the Preliminary Reference Earth Model and a local seismic velocity model. The amplitude and phase of the seasonal variation of the vertical and horizontal geodetic positions can be jointly adjusted only with the layered Earth model, while an elastic half-space model fails, emphasizing the importance of using a realistic Earth elastic structure to model surface displacements induced by surface loading. We demonstrate, based on a formal inversion, that the fit to the geodetic data can be improved by adjusting the layered Earth model. Therefore, the study also shows that the modeling of geodetic seasonal variations provides a way to probe the elastic structure of the Earth, even in the absence of direct measurements of surface load variations.

## 1. Introduction

Geodetic time series recorded by the Global Positioning System (GPS) have revealed that surface load variations can induce measurable surface strain. Variations of surface loading can result from various sources: tidal loading [*Agnew*, 1996, 1997], continental water storage [*Blewitt et al.*, 2001; *Bevis et al.*, 2005; *Van Dam et al.*, 2001; *Davis et al.*, 2004; *Bettinelli et al.*, 2008; *Steckler et al.*, 2010; *Elósegui et al.*, 2003; *Fu and Freymueller*, 2012; *Fu et al.*, 2012; *Wahr et al.*, 2013], ice and snow [*Grapenthin et al.*, 2006; *Matsuo and Heki*, 2010; *Jiang et al.*, 2010], and atmospheric pressure [*Kaniuth and Vetter*, 2006]. The analysis of these signals has attracted much attention. One reason is that GPS can provide a way to monitor mass variations of the hydrosphere or cryosphere which are rather difficult to monitor otherwise. Another reason is that correcting for these variations is important to measure accurately secular geodetic velocities [*Blewitt and Lavallée*, 2002] and to detect eventual aseismic tectonic transients. It has been shown that in some instance, surface load induced deformation had been misinterpreted as tectonic transients or had obscured subtle tectonic transients [*Vergnolle et al.*, 2010]. Finally, the measurements and modeling of the Earth response to surface load variations provide a way to probe the density and elastic structure of the Earth as has been shown recently from the analysis of geodetic deformation induced by oceanic tides [*Ito and Simons*, 2011].

In this study, we focus on the Himalaya region where the monsoon regime induces large variations of continental water storage and where strong seasonal geodetic strain has been documented [*Bettinelli et al.*, 2008; *Steckler et al.*, 2010; *Flouzat et al.*, 2009; *Fu and Freymueller*, 2012]. Variations of continental water storage are actually measurable using satellite gravity measurements provided by the Gravity Recovery and Climate Experiment (GRACE) missions, as shown by *Ramillien et al.* [2008] for example (Figure 1), while geodetic displacements are measured by continuous GPS (cGPS) stations. The Himalaya region is also a place where deformation transients associated with Himalayan tectonics could be occurring but would have remained undetected so far. In a previous study, *Bettinelli et al.* [2008] have modeled the geodetic strain expected from surface load annual variations, as determined from GRACE, and assuming an elastic half-space. They

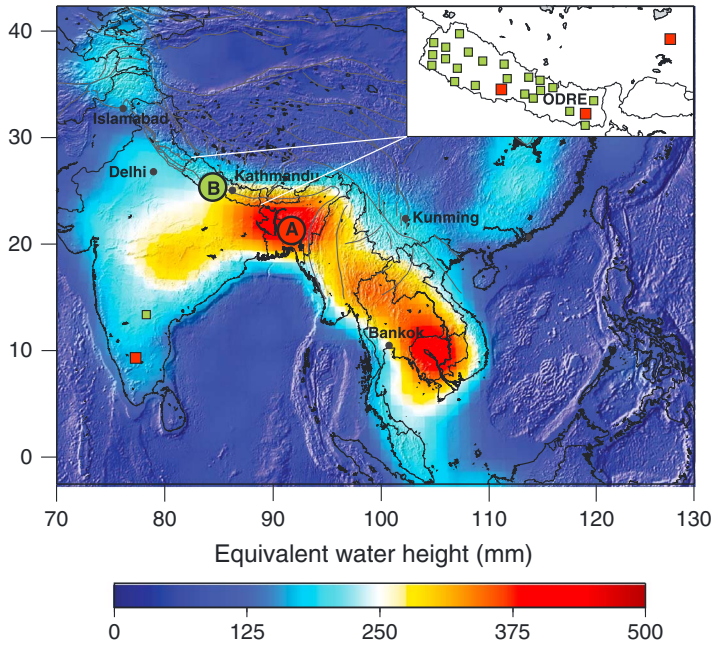


**Figure 1.** Peak to peak surface load variations, expressed in equivalent water height (in mm), derived from GRACE for the 2002–2012 period, and corrected from earthquake coseismic and postseismic contributions. Green dots show location of the cGPS stations used in this study, and red squares highlight the cGPS stations for which time series are plotted in Figures 2 and 6. Circles labeled A and B show location of the surface load time series of Figure 3. Point A, in Bangladesh, is located approximately where the seasonal variation is maximum.

found a relatively good fit with the GPS seasonal signal but noticed a difficulty to match simultaneously the amplitude and phase of the vertical and horizontal components. They were using data from a single transect across the Himalaya at the longitude of Kathmandu. This problem is even more conspicuous when data from cGPS stations more widely distributed over the Nepal Himalaya and India are considered (Figure 2). Here we investigate further that issue and show that the amplitude and phase of the vertical and horizontal components of the seasonal strain are explained significantly better if a PREM (Preliminary Reference Earth Model) layered spherical Earth model is considered rather than an elastic half-space. We then exploit geodetic displacements induced by seasonal variations of continental water storage to constrain a shallow depth-dependent PREM-like regional model. In the following we present first the GPS and GRACE data analyzed in this study and then our modeling and inversion results.

## 2. Presentation of the GPS and GRACE Data Used in This Study

### 2.1. The GPS Data Set

We use data from three International GNSS Service (IGS) stations available in the study area and from the Geodetic network of Nepal (see locations of stations in Figure 1). The Nepal network consists of three cGPS stations, which were installed in 1997 under a collaboration between the Laboratoire de Détection et Géophysique (CEA/LDG, France) and the Department of Mines and Geology (DMG, Nepal), and 25 stations which were deployed since 2003 by the Tectonics Observatory (http://www.tectonics.caltech.edu). The daily station positions in ITRF2005 were computed from 24 h GPS dual-frequency phase and code observations with the GAMIT/GLOBK processing software in a two-step procedure [*King and Bock*, 2005; *Herring*, 2005]. We used the Global Mapping Function model for the tropospheric mapping function [*Boehm et al.*, 2006] and estimated horizontal tropospheric gradients at each station. We include data sampled at a 2 min interval from reference stations DGAR, GUAM, GUAO, HYDE, IISC, KUNM, LHAS, LHAZ, POL2, SELE, URUM, and WUHN to obtain a very loosely constrained regional solution. Satellite orbital parameters used were those published by IGS as final. The regional solution was combined with solutions at the normal equation level from five global IGS subnetworks (Scripps Orbit and Permanent Array Center IGS1 through IGS5) to arrive at final site positions. The detrended time series, after removal of a best fitting linear trend, are shown in Figure 2 for four continuous GPS stations. The error

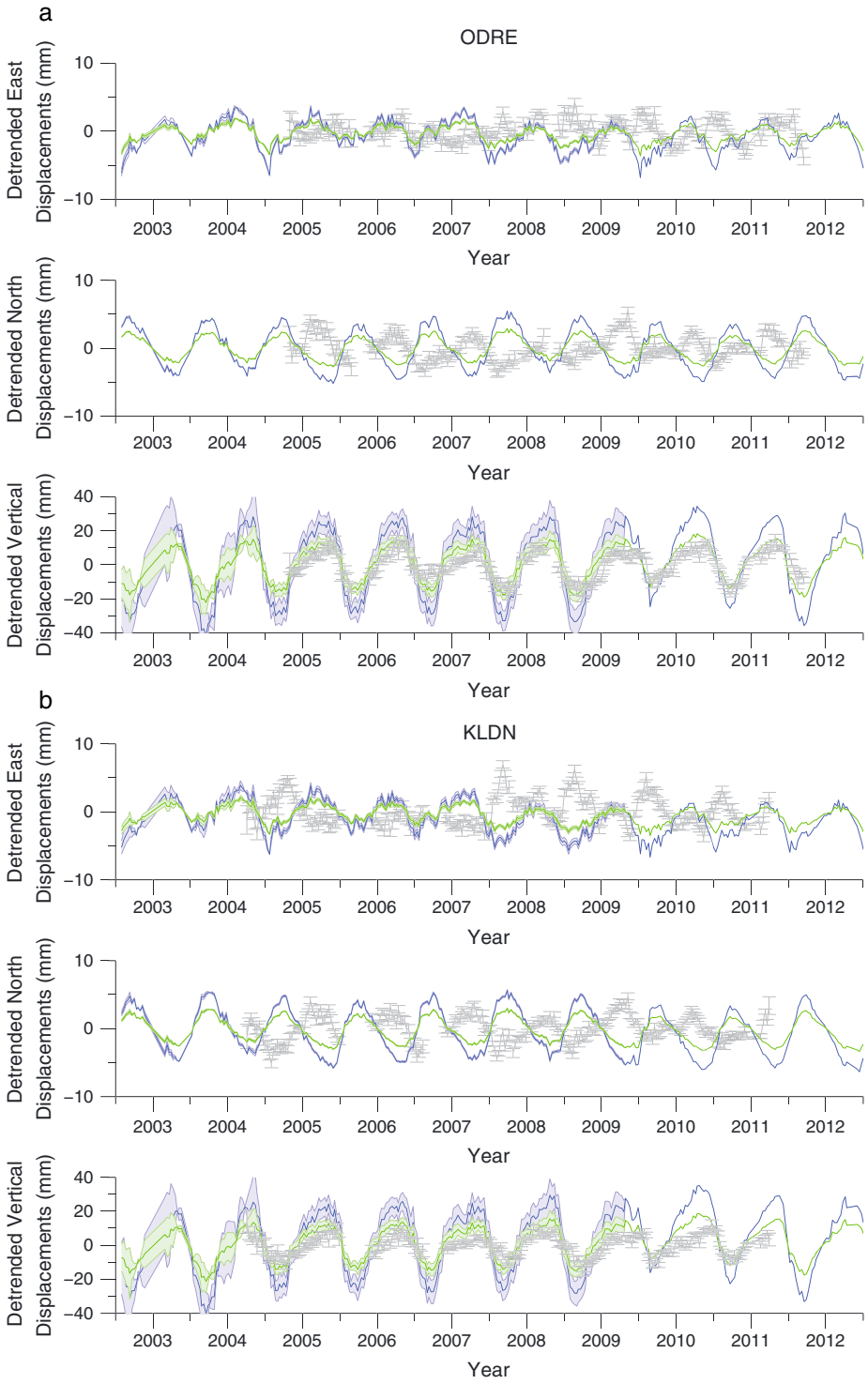


**Figure 2.** Detrended geodetic positions, averaged over 10 days, determined at stations (a) ODRE, (b) KLDN, (c) LHAZ, and (d) IISC (gray symbols). See Figure 1 for locations of these stations. Error bars show 1$\sigma$ uncertainties. The green and blue lines show predicted surface displacements computed from surface load variations derived from GRACE assuming a homogeneous elastic half-space. Blue line corresponds to a Young's modulus $E$ of 90 GPa, the value found to yield the best overall fit to the horizontal components (Table 1). Green line corresponds to a Young's modulus $E$ of 170 GPa, the value found to yield the best overall fit to the vertical component (Table 1). Poisson's ratio, $\nu$, is 0.25 for both models. Shaded areas show uncertainties on predictions derived from uncertainties on estimated surface loads.

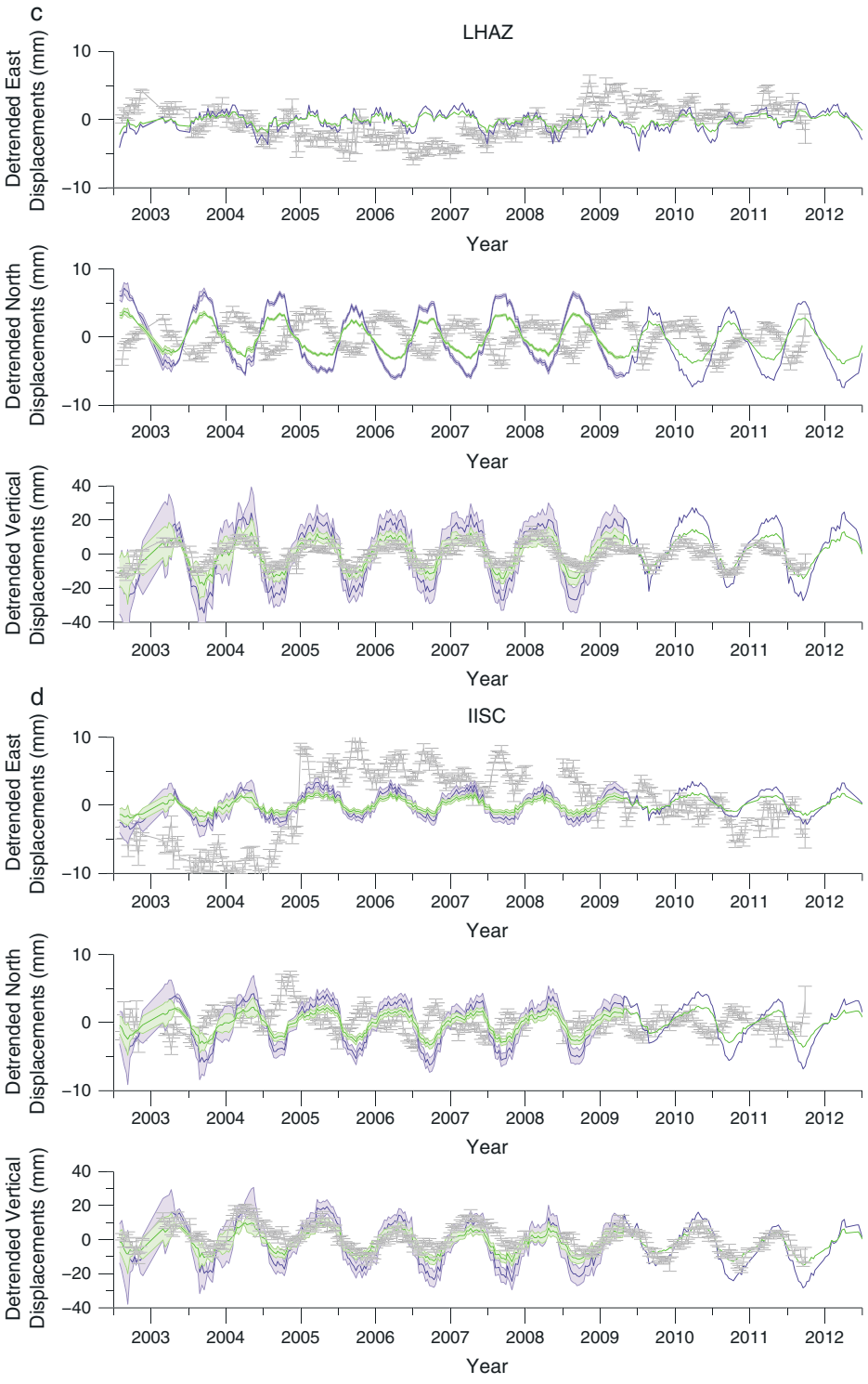


**Figure 2.** (continued)

bars represent formal 1 standard deviations derived from the Kalman filter solution of the joint networks (Nepal regional network plus IGS1 through IGS5). They rely on tight position constraints for the IGS reference sites and assume that monument noise is white (Flicker noise is not accounted for). These time series show strong seasonal variations at all stations. The gray dots and error bars represent a 10 day averaged signal used to reduce the daily scatter. The location of the three stations are plotted in Figure 1.

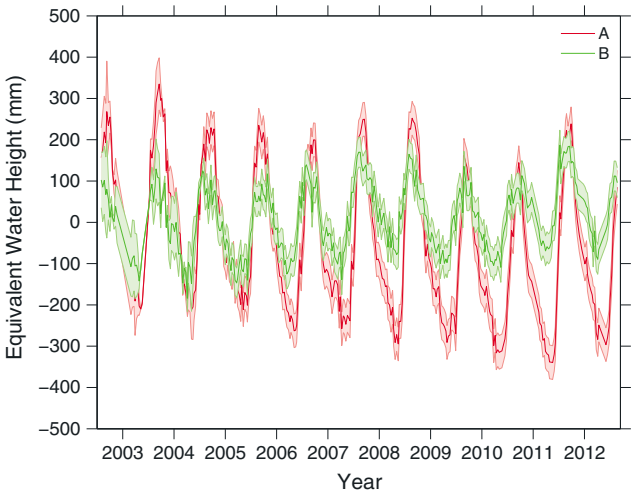


**Figure 3.** Surface load variations at locations of points A (red line) and B (green line) reported in Figure 1. Note that surface load variations at point B, in the Nepal Himalaya, is shifted by about 2 months with respect to the time series at point A in Bangladesh. Shaded areas represent the final uncertainty on regional water mass averages from (1) formal errors from processed Stokes coefficients adjustment; (2) inside leakage error induced by very dominant hydrological signals from outside of the studied area, up to 10 cm of equivalent water height on the signal amplitude at our GPS stations (e.g., important water mass change drainage basins); and (3) outside leakage error or uncertainties due to the spectrum truncation up to cutoff degree 50 (yielding a spatial resolution of 300–400 km) that could represent up to 6% of the estimate of equivalent water height [*Ramillien et al.*, 2005, 2006, 2008].

### 2.2. Continental Water Mass Variations Derived From GRACE Level-2 Solutions

We are interested in seasonal variations of surface loading driven by surface hydrology. We take advantage of the data collected by the GRACE experiment, a tandem satellite mission launched in March 2002. GRACE provides a global mapping of the gravity field variations from monthly to decade time scales [*Tapley et al.*, 2005] and thus gives access to redistributions of large-scale surface water mass (atmosphere, oceans, and continental water storage) once the static geoid is corrected. Gravitational contributions of the known time-varying phenomena (tides and polar movements) are removed from the raw GRACE measurements, and then monthly and 10 day level 2 solutions are obtained by least squares orbit adjustment of the residual observations for each period of time [*Lemoine et al.*, 2007; *Bruinsma et al.*, 2010]. An atmospheric and nontidal oceanic loads in the GRACE data are not corrected for as they are not accounted for in the GPS processing, using the nontidal ocean model forced by air pressure and wind on ocean: Mog-2D [*Carrère and Lyard*, 2003], provided by the European Centre for Medium-Range Weather Forecasts. We notice, however, that amplitudes of atmospheric and nontidal loading in this region are relatively low (a few mm) compared to the annual variations of continental loading. In this study, we use 10 day solutions provided by the Centre National d'Etudes Spatiales / Groupe de Recherche de Géodésie Spatiale (CNES/GRGS), available at http://grgs.obs-mip.fr/. These solutions are expressed in terms of Stokes coefficients (i.e., nondimensional spherical harmonic coefficients of the geopotential) which represent the gravitational effects of nonmodeled phenomena, mainly continental hydrology (the degree 1 Stokes coefficients have been omitted in our study). The solutions also contain polluting noise, aliasing effects, leakage, and errors in the correction models. Several postprocessing filtering approaches of the residual Stokes coefficients have been proposed to extract realistic continental hydrology signals and to get rid of the high-frequency energetic north-south striping that is due to orbit resonance during the Stokes coefficient determination [*Wagner et al.*, 2006] and aliasing of the not-well-resolved short-term phenomena. Stokes coefficients can be easily converted into geoid and water mass coefficients (expressed in terms of mm of equivalent water height) by isotropic filtering [*Ramillien et al.*, 2005]. Then, 10 day $1° \times 1°$ grids of water mass are simply interpolated from the water mass coefficients, and a time average is removed to each 10 day solution so that the solutions are expressed with respect to the mean solution over the time span of analysis. In our study, we estimate the uncertainty on regional water mass averages up to June 2009 from the following: (1) formal errors from processed Stokes coefficients adjustment; (2) inside leakage error induced by very dominant hydrological signals from outside of the studied area, up to 10 cm of equivalent water height on the signal amplitude at our GPS stations (e.g., important water mass change drainage basins); and (3) outside leakage error or uncertainties due to the spectrum truncation up to cutoff degree 50 (yielding a spatial resolution of 300–400 km) that could represent up to 6% of the estimate of equivalent water height [*Ramillien et al.*, 2005, 2006, 2008]. The errors from spectrum truncation-types (2) and (3) are estimated as a function of time by using an existing global hydrology model (WaterGAP Global Hydrology Model developed by *Döll et al.* [2003]) for our studied region and converting it to GRACE-like observations (with similar spatial resolution, i.e., using Stokes coefficients up to order 50). In addition, we

also suspect errors from correcting models of known gravitational forces, including tides, and time-aliasing effects, but these errors remain difficult to quantify. A logical way to address these uncertainties is to compare different GRACE solutions available from various processing centers, which handle the noise in the L1B satellite observations differently and use different orbit integration methods and different correction models. *Sakumura et al.* [2014] show that differences between four centers (CSR, GFZ, JPL, and GRGS) solutions are small, at least for seasonal variations, of the order 8.3 to 17.6 mm RMS of equivalent water height (compared to the 600 mm amplitude of variation, Figure S1). In addition, these authors show that correlations between solutions decrease with the harmonic degree and are better for middle and small frequencies, i.e., for radial displacements. We conclude that these errors remain small in our area of study, compared to our estimated uncertainties.

In this study, we use continental water variations time series from February 2002 to August 2012 (Figure 1). In this region, tectonic signals represent another source of error. Indeed, *Han et al.* [2006] reported the detection by GRACE of large coseismic gravity changes due to the 2004 $M_w$9.3 Sumatra-Andaman earthquake. Postseismic recovery of the geoid depression is also observed [*Han et al.*, 2008; *Ogawa and Heki*, 2007] and causes apparent variations in equivalent water height [*Chen et al.*, 2007]. Moreover, *Sun and Okubo* [2007] have shown that measurable coseismic and postseismic geoid and gravity changes can be induced by large earthquakes ($M \geq 7.5$). For the purpose of our study, we empirically model and remove earthquake-induced mass redistribution observable in the gravity field measurements of each $M > 7.5$ which occurred within the 2002–2012 period ($M$9.1 December 2004 Sumatra-Andaman; $M$8.5, 7.9, and 7.1 October 2007 Sumatra sequence; and $M$ 7.8 April and $M$ 7.7 October 2010 Sumatra earthquakes), using the following empirical formulation:

$$h_s(m,t) = h(m,t) - \sum_i \alpha_i \mathcal{H}(t-t_i) + \sum_i \beta_i \mathcal{H}(t-t_i) \ln\left(1 + \frac{1-t_i}{\tau}\right), \quad (1)$$

where $h_s$ refers to the seasonal equivalent water height measured by GRACE at point $m$ at the Earth surface, after earthquake contributions have been removed from the equivalent water height $h$. $\mathcal{H}$ is the Heaviside function representing abrupt coseismic changes of the gravity field at time $t_i$, $\tau$ is the characteristic time of postseismic relaxation described by *Hoechner et al.* [2011], and $\alpha_i$ and $\beta_i$ are constants estimated by a least squares inversion. Figure 1 shows the averaged annual peak to peak amplitude of the equivalent water height (in mm) at the Earth surface for the 2002–2012 time period. Figure 3 presents the spatiotemporal variations of the equivalent water height at the surface. The peak to peak amplitude of seasonal variations reaches a maximum of 70 cm in Bangladesh (red line). The amplitude of the signal decreases westward toward Nepal and shows a phase lag of about 3 to 4 months (green line).

## 3. Modeling of Seasonal Ground Deformation Induced by Surface Load Variations

Let us consider a time-varying distributed surface load expressed in terms of a seasonal equivalent water thickness, $h_s(m,t)$, with density $\rho$, where $t$ is time and $m$ refers to the point location at the Earth surface. We assume a purely elastic deformation so that the superposition principle applies. The assumption of a perfectly elastic Earth model is a good first-order approximation at an annual time scale as the Maxwell time associated with viscous relaxation of the crust and lithosphere ranges from decades (postseismic deformation) to thousands of years (postglacial rebound). The time-varying geodetic displacement $U_i(M,t), i = 1,3$ at a point $M$ is then obtained by convolving the load distribution over a surface $S$ with the Green's functions $G_i(M)$:

$$U_i(M,t) = \rho \int_S h_s(m,t) G_i(M-m) \mathrm{d}m. \quad (2)$$

Here $G_i$ refers to the $i$th component of the geodetic displacement at point $M$ at the Earth surface due to a surface point load, a Dirac function, at the origin. For numerical computation, the Earth surface is meshed and a discrete version of equation (2) is adopted, e.g., the integral in (2) is approximated by a sum over the $1° \times 1°$ GRACE grid. The Green functions must be computed based on assumptions of the elastic structure of the Earth. We first show the results obtained assuming a homogeneous elastic half-space and move next to the case of spherical and layered Earth model.

**Table 1.** Reduced Chi-Squares $\chi_r^2$ (See Equation (6)) Obtained From the Inversion of the Geodetic Time Series (~ 4600 Data Points for Each Displacement Component), Using the Boussinesq Half-Space Approximation[a]

| $\chi_r^2$ | Horizontal | Vertical | Horizontal and Vertical |
|---|---|---|---|
| Half-space ($E = 90$ GPa) | 38.1 | 30.2 | 34.1 |
| Half-space ($E = 170$ GPa) | 42.0 | 17.3 | 29.6 |
| Prem | 16.2 | 12.3 | 14.3 |
| MGrace | 13.7 | 5.1 | 9.4 |

[a]The values in bold are the minimum values obtained when the Young's modulus assigned to the elastic half-space is adjusted so as to best fit either the vertical ($E = 170$ GPa) or the horizontal components ($E = 90$ GPa). $\chi_r^2$ using the Preliminary Reference Earth Model model [*Dziewonski and Anderson*, 1981]. Note that the PREM model yields a better fit to both the vertical and horizontal components. Finally, $\chi_r^2$ using a model based on PREM, MGrace. Material properties for the uppermost 150 km are the results of a probabilistic inversion of seasonal geodetic displacements. Note that MGrace leads to an even better fit to both components.

### 3.1. Modeling of Seasonal Ground Deformation for a Homogenous Elastic Half-Space

A common assumption is that an elastic half-space model would be a satisfying first-order approximation to model surface displacements induced by surface loading [e.g., *Bevis et al.*, 2005; *Grapenthin et al.*, 2006; *Bettinelli et al.*, 2008; *Steckler et al.*, 2010]. The advantage of using that approximation is that the solution is analytical [*Boussinesq*, 1885]. However, it has been well established by *Farrell* [1972] for several decades now that a spherical and layered model is the correct one to model both horizontal and vertical components simultaneously. Considering the number of recent studies still using the Boussinesq approximation, we first present results for elastic homogeneous half-space models and emphasize the difficulty to predict surface displacements induced by surface loading for both components using a single model. Surface displacements of a nongravitating, homogeneous half-space to surface loading are commonly referred to as the Boussinesq's problem, for which the Green's functions are obtained by solving the elastic equilibrium equation. Let $F$ be the norm of a unit mass force applied vertically at the model's surface. We consider a cylindrical coordinates system $(r, \theta, z)$, centered on the force application point. The analytical solution then writes

$$u_R(R,0) = \frac{-F(1-2\nu)(1+\nu)}{2\pi ER}, \tag{3}$$

$$u_\theta(R,0) = 0, \tag{4}$$

$$u_z(R,0) = \frac{-F(1-\nu)(1+\nu)}{\pi ER}, \tag{5}$$

where $R$ is the distance between the observation point and the mass point force, $\nu$ is the Poisson's ratio, and $E$ is the Young's modulus, quantifying the resistance of an elastic body to deformation. By symmetry, $u_\theta = 0$ and all components of surface displacements are independent of $\theta$. In this approach there are only two adjustable model parameters: the Young's modulus and the Poisson's ratio. The sensitivity to the Poisson's ratio is actually negligible so that in practice only the Young's modulus is adjusted and $\nu$ is generally set to a standard value of 0.25, as is the case in this study. To compute the deformation induced by distributed surface load, we convolve the spatial distribution of surface loads derived from GRACE with the Green's functions corresponding to an elastic homogeneous half-space described above. We use the 10 day level 2 solutions, expressed in equivalent water height, and a $1° \times 1°$ grid of mass point forces, covering a $40° \times 60°$ area around the Himalayan region (Figure 1). For consistency the cGPS time series are 10 day averaged. Table 1 shows the best fitting Young's modulus obtained from least squares inversion of the GPS data by minimizing a level 2 norm of the residuals $r_i$, weighted by their nominal uncertainties $\sigma_i$:

$$\chi_r^2 = \frac{1}{n-p}\sum_i \frac{r_i^2}{\sigma_i^2}. \tag{6}$$

The number of degrees of freedom is $(n - p)$, $n$ being the number of observations ($n \sim 4200$ for each displacement component) and $p$ the number of fitted parameters ($p = 1$, the Young's modulus, for half-space

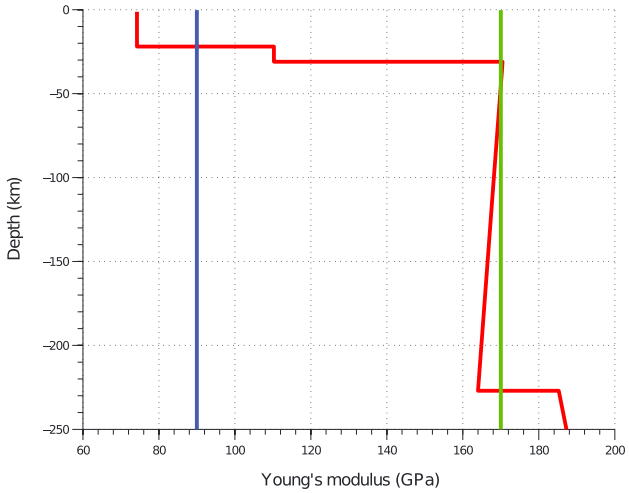


**Figure 4.** Depth variation of the Young's modulus in the modified PREM model used to compute the Green functions for a layered spherical Earth model. The crustal structure is based on the seismic velocity model determined for Nepal by *Monsalve et al.* [2006] (red line). The deeper portion of the model is based on the Preliminary Earth Model [*Dziewonski and Anderson*, 1981]. Also shown is the value of Young's modulus derived from the modeling of vertical (green) and horizontal (blue) seasonal displacements (Table 1).

models, and $p = 0$ for the PREM model). Note that the misfit criterion ignores a possible serial correlation of uncertainties. We find, with no surprise, that if the horizontal and vertical time series are inverted jointly the amplitude of the seasonal variations on the vertical components is systematically underpredicted, while the amplitude of the seasonal variations of the horizontal components is systematically overpredicted. We then look at what Young's modulus is needed in the Boussinesq problem in order to approximate the correct spherical Green's functions for our given load and data distribution. We find best fitting values of the Young's modulus ranging from 92 to 113 GPa for the horizontal components and from 161 to 186 GPa for the vertical components. When all the stations are combined, we find best fitting Young's modulus of ~90 and ~170 GPa for the horizontal and vertical components, respectively. Figure 2 shows 10 day averaged seasonal GPS data in gray and the predicted displacements time series for half-space models with $E = 90$ GPa (blue line) and $E = 170$ GPa (green line). Clearly, as predicted by *Farrell* [1972], the half-space model fails in adjusting simultaneously the amplitude of the seasonal variations of the vertical and horizontal components. This means that the two components have very different sensitivities to the location of the load. The phase is also mispredicted. In particular, it should be noticed that the model predicts a horizontal signal which is clearly out of phase at most stations, being too early by a few months typically, depending on the distance to the load. By contrast, the predicted vertical displacements are approximately in phase with the observations. This could be explained by the fact that given positive loads, the vertical displacements always add constructively, while the horizontal displacements can add destructively depending on the spatial distribution of the load.

### 3.2. Green's Functions for a Spherical, Layered Elastic Earth Model

The Green's functions entering equation (2) can be computed for a spherical perfectly elastic Earth Model based on load Love numbers theory [*Longman*, 1962, 1963; *Farrell*, 1972], in which the deformation of the Earth, generated by a surface load, is a function of the spherical harmonic components of the gravitational potential created by this load. To define the load Love numbers, the vertical and horizontal surface displacements, generated by the surface load, are expanded into spherical harmonics. In this study, the load Love numbers are computed for a model based on PREM [*Dziewonski and Anderson*, 1981], in which the ocean is replaced by a continental crust (Figure 4). We use asymptotic expressions to compute numerically the Legendre series in the Green's functions for the load Love numbers, following *Farrell* [1972] formalism and the numerical method of *Guo et al.* [2004], which is more accurate than the Farrell's original method. The surface Green's functions for vertical and horizontal displacements, induced by a unit mass point force, are then given by

$$u_r = \frac{R}{M}\sum_{n=0}^{\infty} h'_n P_n(\cos\theta), \tag{7}$$

$$u_\theta = \frac{R}{M}\sum_{n=0}^{\infty} l'_n \frac{\partial P_n(\cos\theta)}{\partial\theta}, \tag{8}$$

where $P_n(\cos\theta)$ are the Legendre polynomials of the $n$th degree, $\theta$ is the angular distance between the force application point and the observation point, and $h'_n$ and $l'_n$ are the harmonic coefficients of vertical and horizontal displacement, respectively. $R$ and $M$ denote the radius and mass of the Earth.

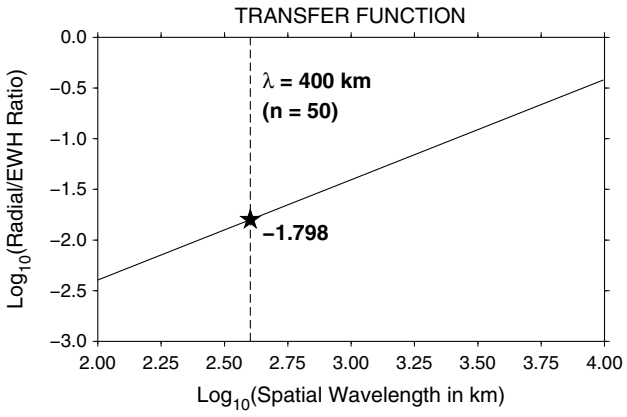


**Figure 5.** Transfer function of the ratio of radial displacement to equivalent water height, as a function of the surface load wavelength. For the resolution of GRACE (~400 km or harmonic degree $n = 50$), the radial surface displacement is 100 times smaller than the applied load. The transfer function favors large wavelength loads, and local hydrology would not significantly affect surface displacements.

Figure 5 shows that displacements at the surface of a spherical nonrotating, elastic, and isotropic Earth, using PREM structure with a continental crust, are mostly controlled by large wavelength loads. Indeed, the evolution of the ratio of radial displacement to the equivalent water height, as a function of the surface load wavelength, highlights that for the resolution of GRACE (~400 km, or harmonic degree of 50), the radial surface displacement is 100 times smaller than the applied load (expressed in equivalent water thickness). The ratio decreases with decreasing load size. Therefore, we will capture the most significant surface displacement with the 400 km resolution of GRACE data.

### 3.3. Comparison of Green's Functions for the Half-Space and Spherical Layered Elastic Earth Models

Figures 6a and 6b represent horizontal and vertical displacements, respectively, computed based on the PREM model described above (red lines) for a point load at origin. The blue and green lines show for comparison the predicted displacements assuming homogeneous half-space models with $E = 90$ GPa (the value found to best fit the horizontal geodetic seasonal displacements) and $E = 170$ GPa (the value found to best fit the vertical geodetic seasonal displacements). These figures, in agreement with *Farrell* [1972] results, help visualize that it is not possible to approximate satisfactorily the layered Earth model with an elastic half-space even if only one single component (vertical or horizontal) is considered. For example, when only the horizontal displacements are considered, the PREM model predicts approximately the same response as a half-space model with $E = 90$ GPa for only a relatively narrow range of distances around ~30 km (−0.5°). When the vertical displacements are considered, this same approximation is valid only at distances of ~3 km (−1.5°). Figure 6c shows the ratio between horizontal and vertical displacements for the PREM model in red (note that this figure could be deduced from *Farrell* [1972] and is in agreement with *Wahr et al.* [2013]). This ratio is constant for an elastic half-space (blue line) and depends only on the Poisson ratio as it is equal to $(1 - 2\nu)/(1 - \nu)$ (see equations (3)–(5)). This shows that if one aims at fitting both the horizontal and vertical components, the variations of sensitivity of the components with the distance to the load must be taken into account. This effect explains why fitting the vertical components with an elastic half-space requires a Young's modulus of 170 GPa significantly larger than the value of 90 GPa inferred from fitting the horizontal components: the two components have different sensitivity to the elastic structure with distance to the load. The Boussinesq model matches the ratio of horizontal to vertical displacements of the PREM model most closely on average for $(1 - 2\nu)/(1 - \nu) \sim 0.44$, i.e., $\nu \sim 0.35$. However, even when this ad hoc value is chosen, it does not help reconciling entirely the amplitude of horizontal and vertical displacements. This is due to the specific distribution of the cGPS stations relative to the load distribution. As a result, best fitting Young's modulus for the horizontal and vertical components are of ~60 GPa and ~140 GPa, respectively, underestimating the horizontal displacements observed at cGPS stations and overestimating the vertical ones. We show in the next section that this effect explains indeed well the relative amplitudes and phase of the vertical and horizontal surface deformation induced by seasonal variations of surface loading in the Himalayan region.

### 3.4. Modeling of Seasonal Ground Deformation for a Spherical, Layered Earth Model

We now compute seasonal surface deformation by convolving the spatial distribution of surface loads derived from GRACE with the Green's functions derived for a spherical, layered Earth model described above. The predicted displacements now fit both the horizontal and the vertical components quite well (Figure 7). The reduced $\chi^2$ of the residuals is reduced by 50% (Table 1). This model thus reconciles the relative amplitudes of the horizontal and vertical components as well as their apparent phase shift and

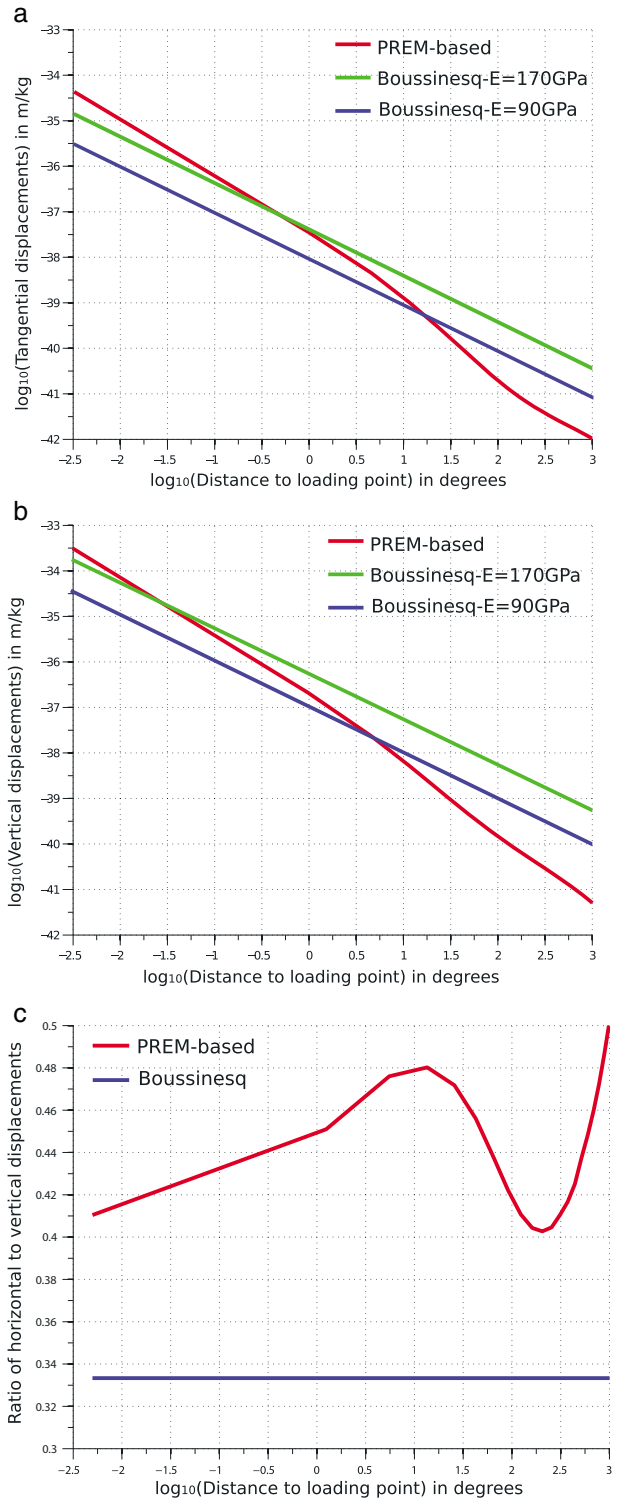


**Figure 6.** (a) Tangential and (b) vertical surface displacements Green's functions for the modified PREM model of Figure 4. Blue and green lines show Green's functions for tangential displacements computed for a homogeneous half-space model with a Young's modulus of 90 GPa and 170 GPa, respectively. The Poisson's ratio is set to 0.25 for all models. (c) Ratio of horizontal and vertical surface displacements Green's functions for the modified PREM model of Figure 4 (red line) and for a homogeneous half-space with a Poisson's ratio of 0.25 (blue line).

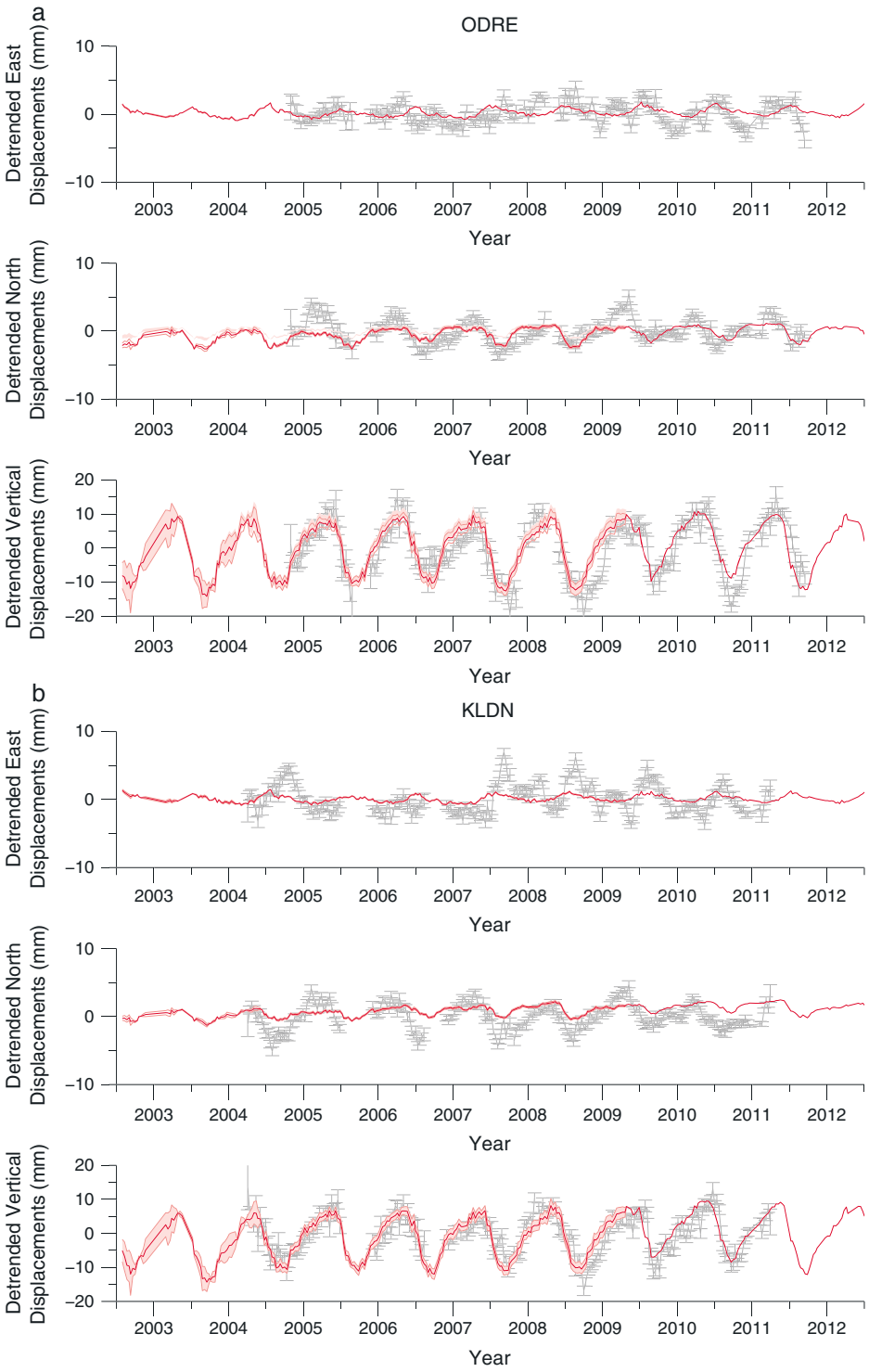


**Figure 7.** Detrended geodetic positions, averaged over 10 days, determined at stations (a) ODRE, (b) KDLDN, (c) LHAZ, and (d) IISC (gray symbols). See Figure 1 for locations of these stations. Error bars show 1$\sigma$ uncertainties. The red line shows predicted surface displacements computed from the surface load variations derived from GRACE assuming the spherical and layered Earth model described in Figure 4. Shaded areas show the uncertainties on the predictions derived from the uncertainties on the estimated surface loads.

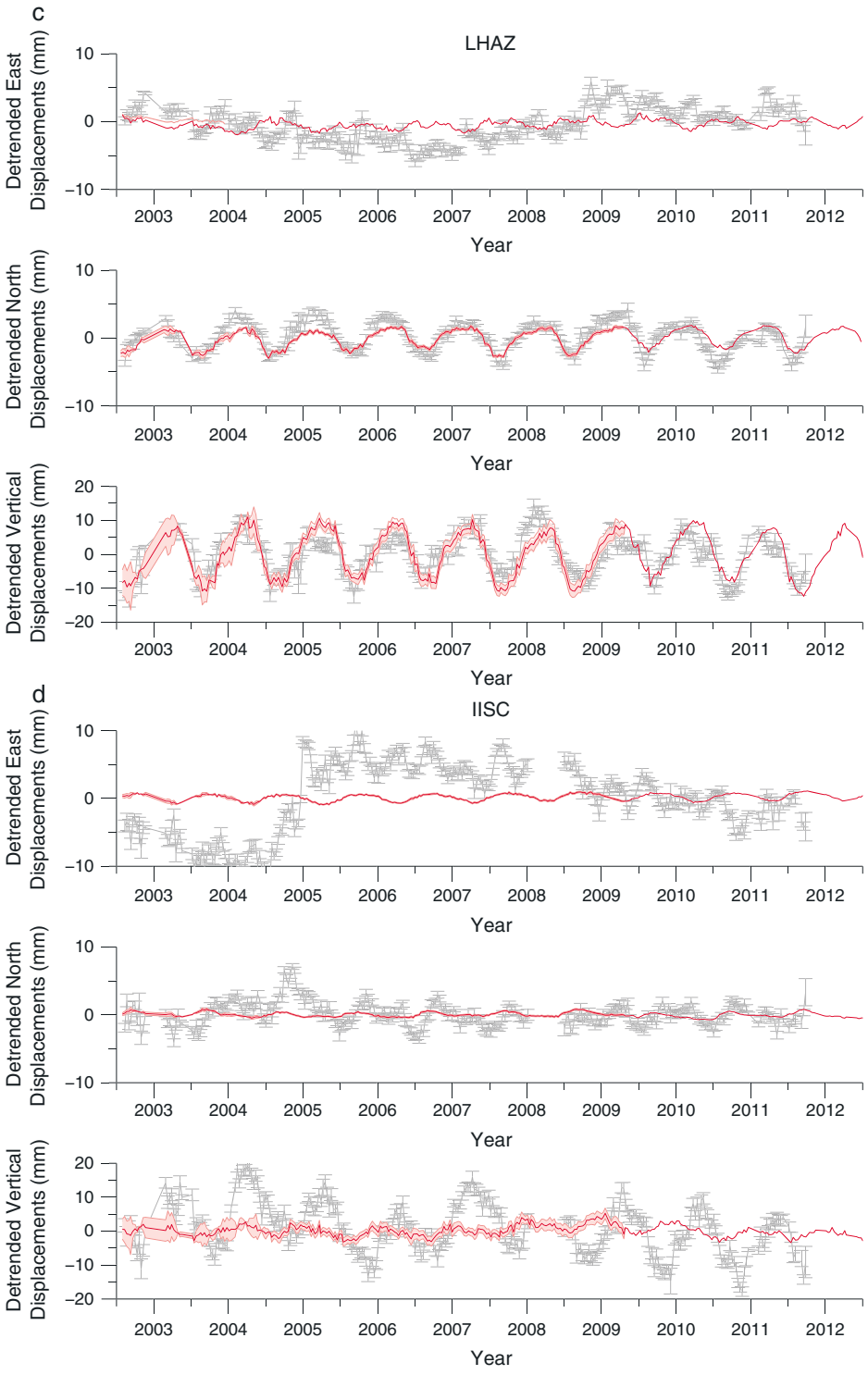


**Figure 7.** (continued)

shape. It is interesting to note that the model fits the GPS data actually better than the elastic half-space models even when only the vertical or the horizontal components are considered (Table 1). In comparison to the $E = 90$ GPa half-space model, the fit to the east component is improved on average by 24% (between 5 and 32% depending on the station considered) and the fit to the north component by 40% (between 12 and 64%). In comparison to the $E = 170$ GPa half-space model, the fit to the vertical data is improved

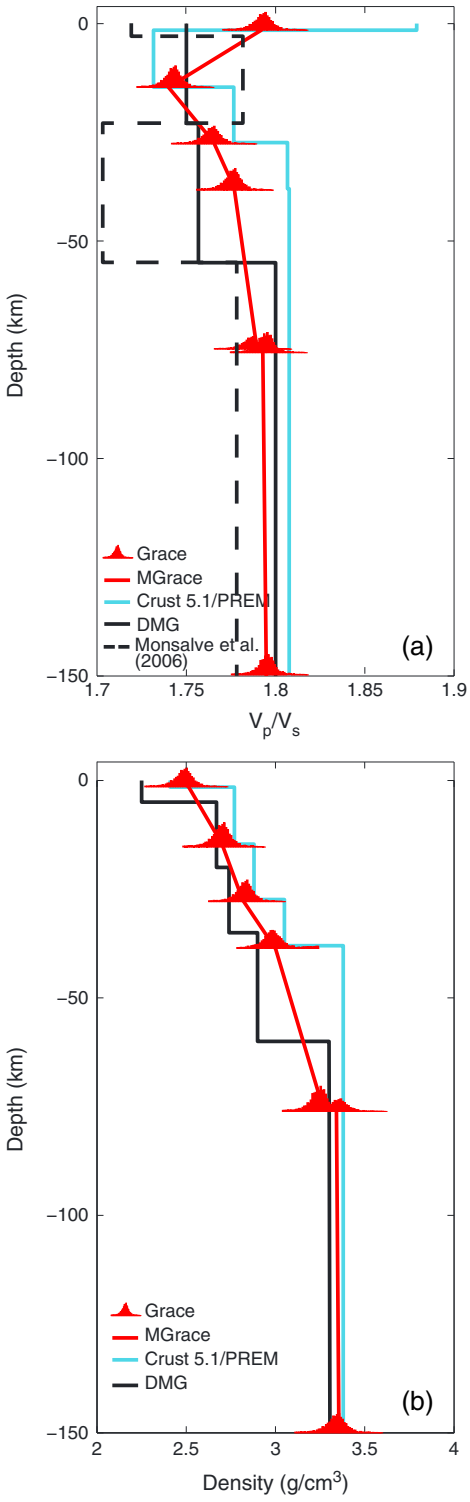


**Figure 8.** Comparison of 1-D models for *P* wave/*S* wave (a) velocities ratio and (b) density of the upper 150 km of the Earth: Crust 5.1/PREM (blue), regional models (solid black from *Pandey et al.* [1995], dashed black from *Monsalve et al.* [2006]), Grace (red histograms represent marginal posterior probability density functions), and MGrace, median derived from Grace.

by 15% (between 2 and 36%). This is clear indication that the dependency of the Green's functions on distance to the load predicted by the modified PREM model is more appropriate than the 1/*R* dependency predicted by the half-space model. The phase shift between the horizontal and vertical components arises from the fact that both displacements are sensitive to different distances to the load. It follows that significant subsidence starts at the onset of the monsoon season as surface loading increases over Bangladesh, but horizontal southward displacements occur only later as the surface load becomes significant in the Gangetic basin immediately to the south of the Nepal Himalaya. Due to the time-varying distribution of surface load induced by the monsoon, combined with the different decrease with distance of their related Green functions, the PREM and the elastic half-space models yield quite different temporal evolution of geodetic displacements. Clearly, the shape predicted by the PREM model fits the geodetic observations better, and the model does improve significantly the fit to most of the seasonal geodetic variations analyzed in this study, but the residuals remain larger than uncertainties on average (Table 1). This could be due partly to underestimated uncertainties on the GPS data, but the misfits show a seasonal residual signal at most stations suggesting the modeling could be improved. These residuals could be due to heterogeneities of surface load distribution, at a scale not resolved by GRACE, or to a nonoptimal elastic Earth structure. We notice furthermore that the fit of our model to the geodetic displacements at station IISC (Figure 7d) is not significantly better than with the Boussinesq model. This station, located in South India, is probably more sensitive to tides (corrected with GAMIT/GLOBK, assuming a tidal model) and nontidal oceanic loading as it is closer to the ocean than the Nepal stations. Even though we take into account the nontidal oceanic load variations forced by the atmosphere, the oscillating load might be biased by other oceanic currents. Another less probable hypothesis is that the PREM Earth structure we used is more appropriate for the Himalayan region than for the Indian craton. In the latter case, modeling of seasonal geodetic strain might be a way to constrain regional variations of elastic properties of the Earth at shallow depths. We therefore propose to solve this inverse problem, in a probabilistic way, and constrain the shallow material properties of the Earth to improve the prediction of seasonal geodetic displacements induced by variations in surface hydrology.

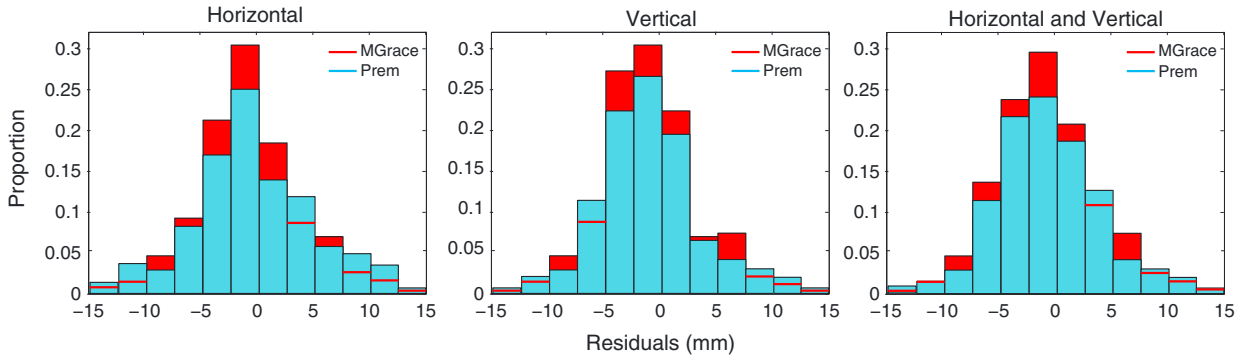


**Figure 9.** Histograms of residuals of seasonal geodetic displacements using Crust 5.1/PREM (blue) and MGrace (red) for horizontal, vertical, and both components.

## 4. Constraining the Crust Depth-Dependent Elastic Structure Using Geodetic Seasonal Surface Displacements

Several previous studies have used tidal records to probe the Earth's structure [*Pariisky*, 1965; *Mantovani et al.*, 2005]. Recently, *Ito and Simons* [2011] used geodetic displacements induced by tidal ocean loading recorded by a dense array of continuous GPS stations in the Western U.S. They inverted this data set, using a fully probabilistic approach, to estimate depth-dependent interior density and elastic moduli and propose a 1-D regional radial structure model, significantly improving the prediction of surface displacement induced by tidal loading. We adopt the same approach, using seasonal geodetic displacements induced by variations in continental water storage. Our initial model is a combination of PREM and a continental crust based on the CRUST 5.1 model [*Mooney et al.*, 1998], which fairly well predicts seasonal geodetic displacements (Figure 9). We parameterize the inverse problem in terms of the ratio between the compressional and shear wave velocities, $V_p/V_s$, and the density $\rho$. We first test the sensitivity of our model by evaluating the effect of small variations of $V_p/V_s$ and $\rho$ on surface radial and tangential displacements, following the method proposed by *Ito and Simons* [2011]. We find that our model is sensitive to the uppermost 150 km of the Earth. Thus, we define $m$, a vector of 14 model parameters consisting of $(\rho, V_p/V_s)$ for each of the seven layers shallower than 150 km and force deeper parameters to be equal to their PREM values. We then evaluate the equation

$$d = G(m) + \epsilon, \tag{9}$$

where $d$ is the seasonal geodetic data vector, $G$ the kernel matrix, and $\epsilon$ the vector of errors on observations, with a Gaussian distribution. We adopt a probabilistic approach, where the posterior probability density function (PDF) is the result of a likelihood function based on the misfits to observations. We use a Bayesian formulation to solve the inverse problem and a Markov Chain Monte Carlo sampling method, with a Metropolis algorithm, to obtain the posterior PDFs of the unknown parameters $(V_p/V_s)$ and $\rho$ [*Tarantola*, 2005]. Figures 8a and 8b show, respectively, PDFs of $(V_p/V_s)$ and $\rho$ for each layer, and the following models: median MGrace from this study, PREM, and two local velocity models [*Pandey et al.*, 1995; *Monsalve et al.*, 2006]. Our density profile shows lower values than the 1-D averaged global model, also in agreement with *Wang et al.* [2013] results, using an inversion of water mass anomalies. The $(V_p/V_s)$ profile is closer to the local velocity model found by *Pandey et al.* [1995] than the Crust 5.1/PREM model but does not capture the low $(V_p/V_s)$ zone between 23 and 55 km found by [*Monsalve et al.*, 2006]. Figure 9 shows histograms of residual seasonal displacements using Crust 5.1/ PREM (in blue) and MGrace (in red) for horizontal, vertical, and both components. MGrace improves significantly the fit to the data by 20% compared to the fit obtained with PREM (Table 1). Note that we are confident that the inversion is not biased by the relatively low resolution of the GRACE data set. Indeed, the transfer function converting surface loads into surface displacements on a spherical Earth weights long wavelengths more heavily (Figure 5). Thus, a loading signal at shorter wavelength than the GRACE resolution would have a negligible effect on the induced surface displacements. It is also possible that the fit to the data could be improved further by allowing for variations of the Earth elastic properties in 3-D. Such an inversion is beyond the scope of this study. The inversion presented here is sufficient to demonstrate the possibility of using seasonal geodetic displacements induced

by surface hydrology to probe the shallow elastic structure of the Earth but requires more data coverage to give significant insights on the Earth local elastic structure.

## 5. Implications and Conclusions

Our study confirms the conclusion of *Bettinelli et al.* [2008] and *Fu and Freymueller* [2012] that the seasonal strain seen in the Himalaya on the horizontal and vertical components is primarily due to surface load variations induced by continental hydrology. The model also explains the seasonal variations seen in Bangladesh [*Steckler et al.*, 2010] as well as in southern India and Tibet as shown in this study. The comparison between the homogeneous elastic half-space and the PREM models shows that vertical and horizontal displacements are sensitive to different distances to the load. As a result, the Young's modulus needed to approximate the correct spherical Green's function using a Boussinesq's approximation from the modeling of vertical displacement is typically of the order of 110 to 190 GPa as found in this and other studies [*Bevis et al.*, 2005; *Steckler et al.*, 2010], while horizontal displacements are better adjusted with significantly lower Young's modulus, 92 to 113 GPa in this study. Also, the value of the Young's modulus derived from inverting geodetic time series based on the Boussinesq's approximation depends on the spatial distribution of the stations, with respect to the distribution of surface load. This problem is solved when a spherical layered Earth model is considered, as demonstrated by *Farrell* [1972]. The PREM model is also found to reproduce better the temporal structure of the signal seen on individual components in our data set as the seasonal loading pattern induced by the monsoon is not stationary. This improvement is due to a better account of dependency of surface deformation to the distance to the load point. The study thus points to the importance of using a realistic model of the elastic Earth structure to model deformation induced by surface loads. It also shows the possibility to use seasonal geodetic displacements induced by variations in continental hydrology recorded by GRACE to probe the shallow Earth elastic structure (at depths typically shallower than 150 km). We show that the density profile found by inverting seasonal variations of surface displacements induced by continental hydrology shows lower density values for the crust, similar to a local density model. $(V_p/V_s)$ profile derived from GRACE is in agreement with one of the local velocity models but lacks at reproducing a lower $(V_p/V_s)$ zone between 23 and 55 km found by *Monsalve et al.* [2006]. Our study also has implications for tectonic geodesy as the accurate determination of secular rates, as well as the detection of transient deformation events, requires proper identification and modeling of nontectonic sources of surface deformation. Finally, the study shows that to probe the depth-dependent shallow Earth structure properties from the response to surface load variations, it is advantageous to use both the vertical and horizontal components. Therefore, we propose a code written in Matlab to compute surface horizontal and vertical displacements at GPS stations due to atmospheric, nontidal oceanic loads (MOG-2D) and residual surface loads (continental hydrology, sediment transport...) inferred from GRACE. The code is available on the Tectonics Observatory's website (http://www.tectonics.caltech.edu/).

**Acknowledgments**

This research was funded by the Gordon and Betty Moore Foundation through the Tectonics Observatory at Caltech and by NSF grant EAR-0838495. We thank John Galetzka and all our collaborators at Laboratoire de détection et géophysique (CEA/LDG, France) and the Nepal Seismological Center and the Department of Mines and Geology (Nepal), for their contribution to the deployment, maintenance, and operation of the cGPS stations used in this study. We are indebted to Takeo Ito for introducing K.C. to the computation of the Green functions for a spherical Earth model. This is a Tectonics Observatory contribution. We also thank Jeff Freymueller and one anonymous reviewer for thorough and helpful reviews, as well as Duncan Agnew for comments on an early version of this manuscript.

## References

Agnew, D. (1996), SPOTL: Some programs for ocean-tide loading. SIO Reference Series 96-8, Scripps Institution of Oceanography.

Agnew, D. (1997), NLOADF: A program for computing ocean-tide loading, *J. Geophys. Res.*, *102*, 5109–5110.

Bettinelli, P., J.-P. Avouac, M. Flouzat, L. Bollinger, G. Ramillien, S. Rajaure, and S. Sapkota (2008), Seasonal variations of seismicity and geodetic strain in the Himalaya induced by surface hydrology, *Earth Planet. Sci. Lett.*, *266*, 332–344.

Bevis, M., D. Alsdorf, E. Kendrick, L. P. Fortes, B. Forsberg, R. Smalley Jr., and J. Becker (2005), Seasonal fluctuations in the mass of the Amazon River system and Earth's elastic response, *Geophys. Res. Lett.*, *32*, L16308, doi:10.1029/2005GL023491.

Blewitt, G., and D. Lavallée (2002), Effect of annual signals on geodetic velocity, *J. Geophys. Res.*, *107*(B7), 2145, doi:10.1029/2001JB000570.

Blewitt, G., D. Lavallee, P. Clarke, and K. Nurutdinov (2001), A new global mode of Earth deformation: Seasonal cycle detected, *Science*, *294*, 2342–2345.

Boehm, J., A. Niell, P. Tregoning, and H. Schuh (2006), Global Mapping Function (GMF): A new empirical mapping function based on numerical weather model data, *J. Geophys. Res.*, *33*, L07304, doi:10.1029/2005GL025546.

Boussinesq, J. (1885), Application des potentiels à l'étude de l'équilibre et du mouvement des solides élastiques, Gauthier-Villars.

Bruinsma, S., J.-M. Lemoine, R. Biancale, and N. Valès (2010), CNES/GRGS 10-day gravity field models (release 2) and their evaluation, *Adv. Space Res.*, *45*(4), 587–601.

Carrère, L., and F. Lyard (2003), Modeling the barotropic response of the global ocean to atmospheric wind and pressure forcing-comparisons with observations, *Geophys. Res. Lett.*, *30*(6), 1275, doi:10.1029/2002GL016473.

Chen, J. L., C. R. Wilson, B. D. Tapley, and S. Grand (2007), GRACE detects coseismic and postseismic deformation from the Sumatra-Andaman earthquake, *Geophys. Res. Lett.*, *34*, L13302, doi:10.1029/2007GL030356.

Davis, J. L., P. Elósegui, J. X. Mitrovica, and M. E. Tamisiea (2004), Climate-driven deformation of the solid Earth from GRACE and GPS, *Geophys. Res. Lett.*, *31*, L24605, doi:10.1029/2004GL021435.

Döll, P., F. Kaspar, and B. Lehner (2003), A global hydrological model for deriving water availability indicators: Model tuning and validation, *J. Hydrol.*, *270*(1-2), 105–134.

Dziewonski, A., and D. Anderson (1981), Preliminary reference Earth model, *Phys. Earth Planet. Inter.*, *25*, 297–356.

Elósegui, P., J. L. Davis, J. X. Mitrovica, R. A. Bennett, and B. P. Wernicke (2003), Crustal loading near Great Salt Lake, Utah, *Geophys. Res. Lett.*, *30*(3), 1111, doi:10.1029/2002GL016579.
Farrell, W. (1972), Deformation of the Earth by surface loads, *Rev. Geophys.*, *10*, 761–797.
Flouzat, M., P. Bettinelli, P. Willis, J. Avouac, T. Héritier, and U. Gautam (2009), Investigating tropospheric effects and seasonal position variations in GPS and DORIS time-series from the Nepal Himalaya, *Geophys. J. Int.*, *178*(3), 1246–1259.
Fu, Y., and J. T. Freymueller (2012), Seasonal and long-term vertical deformation in the Nepal Himalaya constrained by GPS and GRACE measurements, *J. Geophys. Res.*, *117*, B03407, doi:10.1029/2011JB008925.
Fu, Y., J. T. Freymueller, and T. Jensen (2012), Seasonal hydrological loading in southern Alaska observed by GPS and GRACE, *Geophys. Res. Lett.*, *39*, L15310, doi:10.1029/2012GL052453.
Grapenthin, R., F. Sigmundsson, H. Geirsson, T. Árnadóttir, and V. Pinel (2006), Icelandic rhythmics: Annual modulation of land elevation and plate spreading by snow load, *Geophys. Res. Lett.*, *33*, L24305, doi:10.1029/2006GL028081.
Guo, J., Y. Li, Y. Huang, H. Deng, S. Xu, and J. Ning (2004), Green's function of the deformation of the Earth as a result of atmospheric loading, *Geophys. J. Int.*, *159*, 53–68.
Han, S.-C., C. K. Shum, M. Bevis, C. Ji, and C.-Y. Kuo (2006), Crustal dilatation observed by GRACE after the 2004 Sumatra-Andaman earthquake, *Science*, *313*, 658–662.
Han, S.-C., J. Sauber, S. B. Luthcke, C. Ji, and F. F. Pollitz (2008), Implications of postseismic gravity change following the great 2004 Sumatra-Andaman earthquake from the regional harmonic analysis of GRACE intersatellite tracking data, *J. Geophys. Res.*, *113*, B11413, doi:10.1029/2008JB005705.
Herring, T. (2005), GLOBK: Global Kalman filter VLBI and GPS analysis program, Version 10.2, Mass. Inst. of Technol., Cambridge, Mass.
Hoechner, A., S. V. Sobolev, I. Einarsson, and R. Wang (2011), Investigation on afterslip and steady state and transient rheology based on postseismic deformation and geoid change caused by the Sumatra 2004 earthquake, *Geochem. Geophys. Geosyst.*, *12*, Q07010, doi:10.1029/2010GC003450.
Ito, T., and M. Simons (2011), Probing asthenospheric density, temperature, and elastic moduli below the western United States, *Science*, *332*, 947–951.
Jiang, Y., T. Dixon, and S. Wdowinski (2010), Accelerating uplift in the North Atlantic region as an indicator of ice loss, *Nat. Geosci.*, *3*(6), 404–407.
Kaniuth, K., and S. Vetter (2006), Estimating atmospheric pressure loading regression coefficients from GPS observations, *GPS Solutions*, *10*(2), 126–134.
King, R., and Y. Bock (2005), Documentation for the GAMIT GPS Analysis software, release 10.2, Mass. Inst. of Technol., Scripps Inst. of Oceanogr.
Lemoine, J.-M., S. Bruinsma, S. Loyer, R. Biancale, J.-C. Marty, F. Perosanz, and G. Balmino (2007), Temporal gravity field models inferred from GRACE data, *Adv. Space Res.*, *39*, 1620–1629.
Longman, I. (1962), A Green's function for determining the deformation of the Earth under surface mass loads: 1. Theory, *J. Geophys. Res.*, *67*(2), 845–850.
Longman, I. (1963), A Green's function for determining the deformation of the Earth under surface mass loads: 2. Computations and numerical results, *J. Geophys. Res.*, *68*(2), 485–496.
Mantovani, M., W. Shukowsky, S. de Freitas, and B. Brito Neves (2005), Lithosphere mechanical behavior inferred from tidal gravity anomalies: A comparison of Africa and South America, *Earth Planet. Sci. Lett.*, *230*, 397–412.
Matsuo, K., and K. Heki (2010), Time-variable ice loss in Asian high mountains from satellite gravimetry, *Earth Planet. Sci. Lett.*, *290*, 30–36.
Mooney, W. D., G. Laske, and T. G. Masters (1998), CRUST 5.1: A global crustal model at $5° \times 5°$, *J. Geophys. Res.*, *103*(B1), 727–747.
Monsalve, G., A. Sheehan, V. Schulte-Pelkum, S. Rajaure, M. R. Pandey, and F. Wu (2006), Seismicity and one-dimensional velocity structure of the Himalayan collision zone: Earthquakes in the crust and upper mantle, *J. Geophys. Res.*, *111*, B10301, doi:10.1029/2005JB004062.
Ogawa, R., and K. Heki (2007), Slow postseismic recovery of geoid depression formed by the 2004 Sumatra-Andaman Earthquake by mantle water diffusion, *Geophys. Res. Lett.*, *34*, L06313, doi:10.1029/2007GL029340.
Pandey, M. R., R. P. Tandukar, J. P. Avouac, J. Lave, and J. P. Massot (1995), Interseismic strain accumulation on the Himalayan crustal ramp (Nepal), *Geophys. Res. Lett.*, *22*(7), 751–754.
Pariisky, N. (1965), The regional heterogeneity of the mantle as revealed by earth-tide observations, *Tectonophysics*, *1*, 439–442.
Ramillien, G., J. S. Famiglietti, and J. Wahr (2008), Detection of continental hydrology and glaciology signals from GRACE: A review, *Surv. Geophys.*, *29*, 361–374.
Ramillien, G., F. Frappart, A. Cazenave, and A. Güntner (2005), Time variations of land water storage from an inversion of 2 years of GRACE geoids, *Earth Planet. Sci. Lett.*, *235*, 283–301.
Ramillien, G., F. Frappart, A. Güntner, T. Ngo-Duc, A. Cazenave, and K. Laval (2006), Time variations of the regional evapotranspiration rate from Gravity Recovery and Climate Experiment (GRACE) satellite gravimetry, *Water Resour. Res.*, *42*, W10403, doi:10.1029/2005WR004331.
Sakumura, C., S. Bettadpur, and S. Bruinsma (2014), Ensemble prediction and intercomparison analysis of GRACE time-variable gravity field models, *Geophys. Res. Lett.*, *41*, 1389–1397, doi:10.1002/2013GL058632.
Steckler, M. S., S. L. Nooner, S. H. Akhter, S. K. Chowdhury, S. Bettadpur, L. Seeber, and M. G. Kogan (2010), Modeling Earth deformation from monsoonal flooding in Bangladesh using hydrographic, GPS, and Gravity Recovery and Climate Experiment (GRACE) data, *J. Geophys. Res.*, *115*, B08407, doi:10.1029/2009JB007018.
Sun, W., and S. Okubo (2007), Surface potential and gravity changes due to internal dislocations in a spherical earth—I. Theory for a point dislocation, *Geophys. J. Int.*, *114*, 569–592.
Tapley, B., et al. (2005), GGM02–An improved Earth gravity field model from GRACE, *J. Geod.*, *79*(8), 467–478.
Tarantola, A. (2005), *Inverse Problem Theory and Methods for Model Parameter Estimation*, Society for Industrial and Applied Mathematics, Philadelphia, Pa.
Van Dam, T., J. Wahr, P. C. D. Milly, A. B. Shmakin, G. Blewitt, D. Lavallée, and K. Larson (2001), Crustal displacements due to continental water loading, *Geophys. Res. Lett.*, *28*, 651–654.
Vergnolle, M., A. Walpersdorf, V. Kostoglodov, P. Tregoning, J. A. Santiago, N. Cotte, and S. I. Franco (2010), Slow slip events in Mexico revised from the processing of 11 year GPS observations, *J. Geophys. Res.*, *115*, B08403, doi:10.1029/2009JB006852.
Wagner, C., D. McAdoo, J. Klokočník, and J. Kostelecký (2006), Degradation of geopotential recovery from short repeat-cycle orbits: Application to GRACE monthly fields, *J. Geod.*, *80*(2), 94–103.

Wahr, J., S. A. Khan, T. van Dam, L. Liu, J. H. van Angelen, M. R. van den Broeke, and C. M. Meertens (2013), The use of GPS horizontals for loading studies, with applications to northern California and southeast Greenland, *J. Geophys. Res. Solid Earth*, *118*, 1795–1806, doi:10.1002/jgrb.50104.

Wang, H., L. Xiang, P. Wu, H. Steffen, L. Jia, L. Jiang, and Q. Shen (2013), Effects of the Tibetan Plateau crustal structure on the inversion of water trend rates using simulated GRACE/GPS data, *Terr. Atmos. Oceanic Sci.*, *24*(4), 505–512.